LETTERS
PUBLISHED ONLINE: 12 DECEMBER 2010 | DOI: 10.1038/NGEO1039
nature geoscience

Interhemispheric symmetry of the tropical African rainbelt over the past 23,000 years

James A. Collins[1]*, Enno Schefuß[1], David Heslop[1†], Stefan Mulitza[1], Matthias Prange[1], Matthias Zabel[1], Rik Tjallingii[2], Trond M. Dokken[3], Enqing Huang[1], Andreas Mackensen[4], Michael Schulz[1], Jun Tian[5], Michelle Zarriess[4] and Gerold Wefer[1]

The distribution of rainfall in tropical Africa is controlled by the African rainbelt[1], which oscillates on a seasonal basis. The rainbelt has varied on centennial to millennial timescales along with changes in Northern Hemisphere high-latitude climate[2–5], the Atlantic meridional overturning circulation[6] and low-latitude insolation[7] over the past glacial–interglacial cycle. However, the overall dynamics of the African rainbelt remain poorly constrained and are not always consistent with a latitudinal migration[2,4–6], as has been proposed for other regions[8,9]. Here we use terrestrially derived organic and sedimentary markers from marine sediment cores to reconstruct the distribution of vegetation, and hence rainfall, in tropical Africa during extreme climate states over the past 23,000 years. Our data indicate that rather than migrating latitudinally, the rainbelt contracted and expanded symmetrically in both hemispheres in response to changes in climate. During the Last Glacial Maximum and Heinrich Stadial 1, the rainbelt contracted relative to the late Holocene, which we attribute to a latitudinal compression of atmospheric circulation associated with lower global mean temperatures[10]. Conversely, during the mid-Holocene climatic optimum, the rainbelt expanded across tropical Africa. In light of our findings, it is not clear whether the tropical rainbelt has migrated latitudinally on a global scale, as has been suggested[8,9].

The modern-day African rainbelt is a band of precipitation that oscillates seasonally between ~20° N and ~20° S (Fig. 1a, Supplementary Information and Fig. S1). On millennial timescales, the distribution of rainfall in tropical Africa has fluctuated along with Northern Hemisphere high-latitude climate change[2–5], ocean circulation[6] and low-latitude insolation[7]. Climate modelling studies suggest that these influences caused latitudinal migrations of the mean annual position of the rainbelt, with a southward migration of the rainbelt when the North Atlantic region was relatively cold owing either to high-latitude ice cover (that is during the Last Glacial Maximum; LGM; ref. 11) or to a slowdown of the Atlantic meridional overturning circulation (that is during Heinrich Stadial 1; HS1; ref. 12). Conversely, models indicate a northward migration during the mid-Holocene when Northern Hemisphere summer insolation was increased[13].

Available proxy records do not, however, document a clear latitudinal shift in African continental rainfall: recent studies indicate dry conditions in both hemispheres during the LGM (ref. 2) and HS1 (refs 3–6), and wet conditions in both hemispheres during the mid-Holocene[4,7,14]. These observations imply that changes in the range of the seasonal oscillation of the rainbelt[2,14,15] took place. However, most proxy studies are based on a single site[3–5], or on a collection of sites using different proxies[2], preventing a comprehensive view on past changes in the dynamics of the rainbelt. We present a new approach using a north–south transect of eight marine sediment cores that spans from 21° N to 17° S offshore tropical western Africa (Table 1, Fig. 1a) and thus covers the full extent of the rainbelt. This enables us to elucidate the dynamics of the rainbelt at the LGM (19–23 kyr; all ages given as calibrated ages before present), Heinrich Stadial 1 (16–19 kyr) and mid-Holocene (6–8 kyr) compared to the late Holocene (0–2 kyr).

As rainfall in tropical Africa is mostly delivered during the wet season, mean annual rainfall is controlled by the length and intensity of wet season rainfall. The spatial distribution of mean annual rainfall (Fig. 1a), however, mostly reflects wet season length (Fig. 1b) rather than wet season intensity (Fig. 1c). The distribution of C_3 vegetation (trees and shrubs) and C_4 vegetation (grasses and sedges) in tropical Africa[16] (Fig. 1d) is also dependant on the wet season length[17]. On the basis of a robust linear regression between modern-day $\%C_3$ vegetation and both wet season length and mean annual rainfall, we are able to estimate past wet season length and also past mean annual rainfall from past vegetation type (Supplementary Information, Fig. S2). We derive the relative contribution of C_3 and C_4 vegetation to the sediment cores from the stable carbon isotope ratios of *n*-alkanes derived from plant leaf waxes[4,18]: C_3 and C_4 vegetation produce waxes with average $\delta^{13}C$ values of −35.2‰ and −21.7‰, respectively[16]. The plant wax *n*-alkanes are transported to the core sites along with the two sources of terrestrial sediment: wind-blown dust[18] and/or suspended river material[19] (Supplementary Information, Fig. S3).

In general, the vegetation patterns for the LGM and HS1 are similar to each other when compared with the late Holocene (Fig. 2). During both time periods, there was relatively less C_3 vegetation (that is fewer trees relative to grasses) in the source areas of the cores located at 21°–12° N (Sahara desert and Sahel savanna) and 6°–17° S (Congolan rainforest and Angolan/Namibian savanna) compared with the late Holocene. On the basis of $\%C_3$ vegetation values, we determine a weighted mean wet season length for these regions of 3 ± 1 months during the LGM and HS1 (uncertainty is the standard error on the weighted mean,

[1]MARUM—Center for Marine Environmental Sciences and Faculty of Geosciences, University of Bremen, D-28359 Bremen, Germany, [2]Royal Netherlands Institute for Sea Research, 1790 AB Den Burg, Texel, The Netherlands, [3]The Bjerknes Centre for Climate Research (BCCR), Uni Research, N-5007 Bergen, Norway, [4]Alfred Wegener Institute for Polar and Marine Research, D-27568 Bremerhaven, Germany, [5]State Key Laboratory of Marine Geology, Tongji University, Shanghai, 200092, China. †Present address: Research School of Earth Sciences, The Australian National University, Canberra ACT 0200, Australia. *e-mail: jcollins@marum.de.

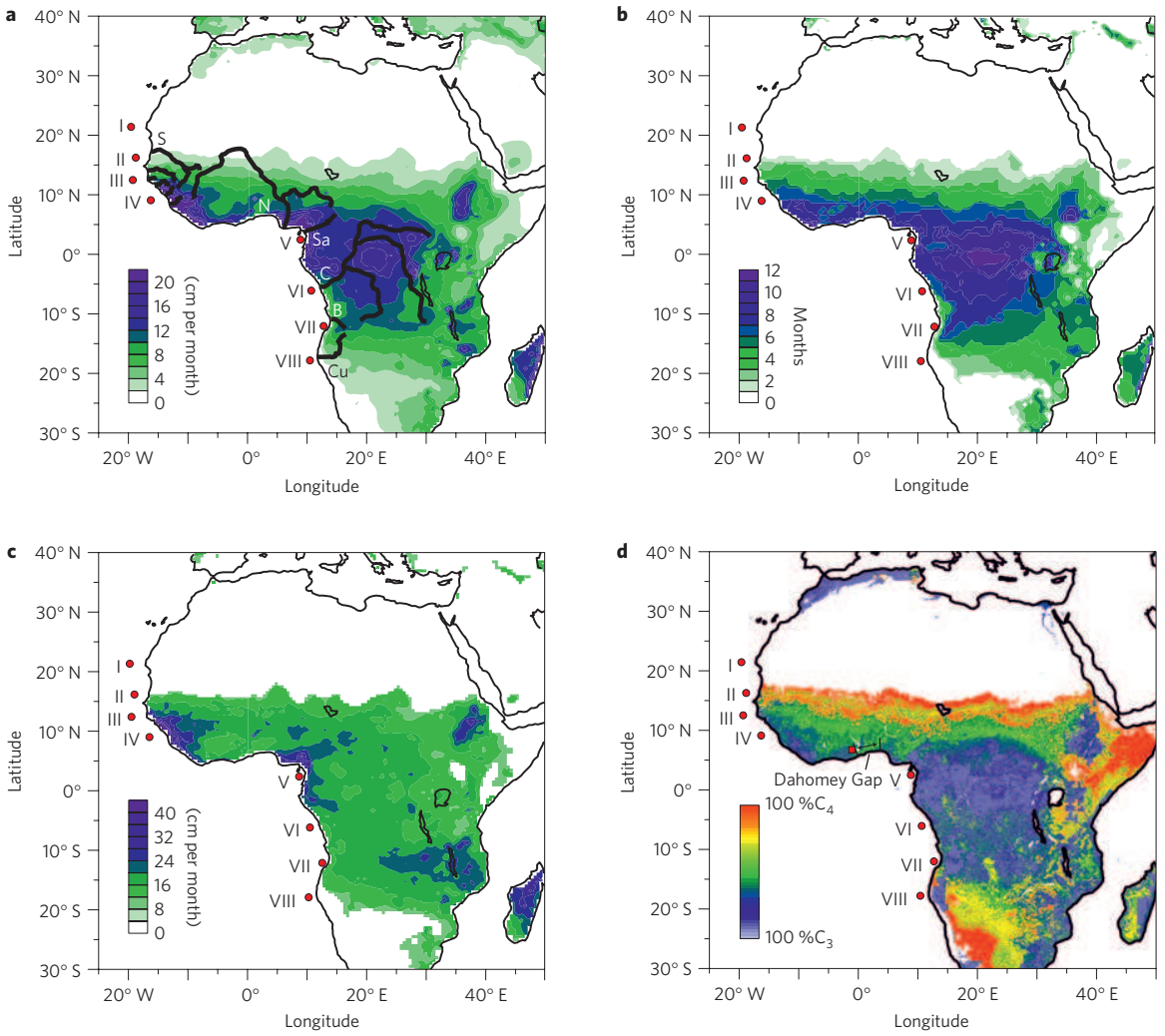

Figure 1 | Modern-day mean annual rainfall, wet season length, wet season intensity and vegetation type for tropical Africa. a, Mean annual rainfall (cm month^{-1}) for the period 1950–1999 (University of Delaware data set; http://climate.geog.udel.edu/~climate/). Senegal (S), Niger (N), Sanaga (Sa), Congo (C), Balombo (B) and Cunene (Cu) rivers are marked, as are smaller West African rivers. Red circles (I–VIII) represent the eight core sites (see Table 1). **b**, Wet season length (number of months exceeding 10 cm month^{-1} rainfall; ref. 17). **c**, Wet season intensity (mean rainfall of months exceeding 10 cm month^{-1} rainfall). **d**, Modern-day vegetation type distribution (ref. 29), ranging between C_3 and C_4 end members. White areas are not vegetated. Lake Bosumtwi (red square) and the Dahomey Gap are marked.

based on 90% prediction intervals; see Supplementary Fig. S2). This is shorter than the corresponding late Holocene value of 4 ± 1 months. The %C_3 vegetation values also indicate mean annual rainfall was 6 ± 1 cm per month during the LGM and HS1 compared with 8 ± 1 cm per month during the late Holocene. In contrast to the decrease in C_3 vegetation in the peripheral regions, the core at 9° N (Guinea–Liberia rainforest region) records the same vegetation type during the LGM and HS1 as the late Holocene, and the core at 2° 30′ N (Cameroon rainforest region) records more C_3 vegetation during the LGM and HS1 (Fig. 2). For the latter region, wet season length was 7 ± 1 months during the LGM and HS1 compared with 6 ± 2 months during the late Holocene, and mean annual rainfall was 12 ± 2 cm per month during the LGM and HS1 compared with 10 ± 4 cm per month during the late Holocene. Similar or wetter conditions in these two regions are in contrast to the low levels of Lake Bosumtwi[20] during the LGM and HS1, suggesting that rainfall in the Dahomey Gap (Fig. 1d) region responded differently to the Guinea–Liberia and Cameroon regions at this time (see Supplementary Information).

To determine whether the vegetation type signal is the result of changing source areas, we also estimate the ratio of wind-blown dust to river-suspended sediment (dust/river) in the sediment core using an unmixing analysis based on major-element composition (Supplementary Information, Fig. S4). Only the LGM and HS1 timeslices exhibit a different overall pattern to the late Holocene. During both of these time periods, there was a large increase in dust/river in the cores at 21°–12° N but a smaller increase in the

Table 1 | Sediment-core transect.

Figure label	Core number	Latitude	Longitude	Water depth (m)
I	GeoB7920-2	20° 45.09′ N	18° 34.90′ W	2,278
II	GeoB9508-5	15° 29.90′ N	17° 56.88′ W	2,384
III	GeoB9526-5	12° 26.10′ N	18° 03.40′ W	3,223
IV	GeoB9535-4	8° 52.54′ N	14° 57.66′ W	669
V	GeoB4905-4	2° 30.00′ N	9° 23.40′ E	1,328
VI	GeoB6518-1	5° 35.30′ S	11° 13.30′ E	962
VII	ODP1078C	11° 55.27′ S	13° 24.02′ E	500
VIII	GeoB1023-5	17° 09.43′ S	11° 00.70′ E	1,978

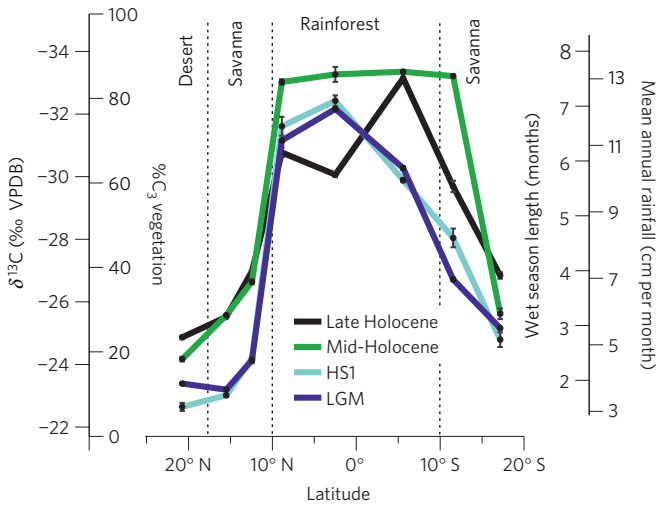

Figure 2 | Latitudinal distribution of vegetation type for modern and past climate states. $\delta^{13}C$ values for the C_{31} plant wax *n*-alkane (‰ VPDB) also quantified as the $\%C_3$ vegetation[16] (that is 100-$\%C_4$ vegetation), plotted against core-site latitude (not source area latitude) for the LGM (19–23 kyr), HS1 (16–19 kyr), mid-Holocene (6–8 kyr) and late Holocene (0–2 kyr). Error bars represent standard error on $\delta^{13}C$ values of all replicates for both samples of each timeslice. $\%C_3$ vegetation is also given in terms of wet season length and mean annual rainfall. Vertical dotted lines mark the approximate boundaries of present-day vegetation zones.

cores at 6°–17° S (Supplementary Fig. S5), in contrast to the relative decrease in C_3 vegetation during the LGM and HS1, which was of a similar magnitude in both hemispheres (Fig. 2). Therefore, we rule out that the decreased relative C_3 contribution can be solely attributed to an increased distal supply of dust from the desert regions. Moreover, other records document drier conditions in the Sahel[21] and a southward shift of the Saharan sand dunes[22] at the LGM, which further supports aridification in the savanna regions rather than increased dust supply from the desert regions.

During the mid-Holocene, the cores at 21°–12° N and 17° S show similar vegetation type to the late Holocene (Fig. 2). Although it is known that the Sahara was wetter than the late Holocene at this time[7], it is thought that mostly savanna (that is C_4) vegetation was dominant in this region during the mid-Holocene[23], which is in line with our results. In contrast to the peripheral regions, C_3 vegetation was highly dominant in the region between 9° N and 12° S during the mid-Holocene (Fig. 2), indicating the existence of dense rainforest. This is supported by pollen records from West[24] and southern-central[25] Africa. Our $\%C_3$ vegetation values suggest that across this region the weighted mean wet season length was 8 ± 1 months during the mid-Holocene compared with 6 ± 1 months during the late Holocene (Fig. 2) and mean annual rainfall was on average 13 ± 2 cm per month during the mid-Holocene compared with 11 ± 2 cm per month during the late Holocene.

The overall vegetation distribution during the LGM and HS1 represents decreased wet season length and mean annual rainfall in the peripheral regions (cores at 21°–12° N and 6°–17° S) and similar or increased wet season length and mean annual rainfall in the equatorial regions (cores at 9° N and 2° 30′ N) relative to the late Holocene. An increase in the portion of the year spent by the rainbelt at equatorial latitudes indicates reduced seasonal oscillation of the rainbelt during the LGM and HS1 compared with the late Holocene. This is in agreement with modelling experiments that suggest that lower global mean temperatures (as during the glacial period; LGM and HS1) were capable of causing such a compression of the atmospheric circulation[10], and this is also in line with other proxy records from southern Africa[26]. However, the mean wet season length of all core sites (21° N–17° S) during the LGM and HS1 (4 months) is shorter than that of the late Holocene (5 months; Fig. 2), indicating a further parameter may have acted to reduce wet season length across the whole range of the rainbelt. Lower global mean temperatures are also capable of reducing atmospheric moisture[27], and therefore we suggest that this acted to reduce the latitudinal width, and possibly the intensity, of the rainbelt throughout the year (see Supplementary Information).

The large increase in aridity in the Sahel region during HS1 relative to the LGM that is documented in other records[6] is not seen here and in other vegetation type records[28], probably because the Sahel was almost entirely C_4 vegetated during the LGM, which would have precluded any further expansion of C_4 vegetation during HS1. For central and southern Africa, however, our results reveal that the slowdown of the Atlantic meridional overturning circulation during HS1 (ref. 6) did not have a large effect on rainfall. This seems to indicate that the overall glacial boundary conditions controlled the rainfall distribution in these regions, rather than the strength of the overturning circulation.

During the mid-Holocene, the overall vegetation distribution indicates increased wet season length across the entire region between 9° N and 12° S relative to the late Holocene. This pattern implies that the latitudinal width, and possibly the intensity, of the rainbelt were increased in this region during the mid-Holocene. As it is known that the rainbelt reached the Sahara[7] and conditions were wetter than the late Holocene at 12° S (Fig. 2), we can also deduce that the seasonal oscillation of the rainbelt was greater during the mid-Holocene. However, the time spent by the rainbelt in the Sahara was probably very brief because the wet season was not long enough to support any large-scale expansion in trees (Fig. 2).

The approximately symmetrical response of the rainbelt between hemispheres is at odds with the rainfall distribution predicted from coupled climate models. The main discrepancy lies in southern-central Africa, where the models do not simulate drier conditions than today during the LGM (ref. 11) or wetter conditions than today during the mid-Holocene[13]. This highlights the need for further modelling and proxy studies in this region. The small difference between HS1 and the LGM in our results is, however, in agreement with freshwater forcing experiments, in terms of the magnitude of the change, which is relatively minor on the African continent compared with the Atlantic Ocean region and South American continent[12]. Overall, our results demonstrate that the hypothesis of a latitudinal shift of the entire rainbelt does not explain rainfall distribution changes in tropical Africa. Although our results do not rule out the possibility that latitudinal shifts of the rainbelt took place over the Atlantic Ocean region[12] and the Asian[9] and South American continents[8], they do raise the question of whether a uniform latitudinal shift is applicable to the entire global tropical rainbelt.

Methods

Age models for the cores are based on published and previously unpublished ^{14}C chronologies (Supplementary Information, Table S1).

Organic analysis was carried out on two samples from each timeslice (three for the late Holocene), taken from approximately the mid-point of the timeslice. Squalane internal standard (10 μg) was added to the samples before extraction. Organic compounds were extracted with a DIONEX Accelerated Solvent Extractor (ASE 200) using a 9:1 mixture of dichloromethane to methanol. Saturated hydrocarbon fractions were obtained using silica column chromatography by elution with hexane and subsequent elution over $AgNO_3$-coated silica to remove unsaturated compounds. Compound-specific $\delta^{13}C$ analyses were carried out using a Thermo Trace GC Ultra coupled to a FinniganMAT 252 isotope ratio monitoring mass spectrometer via a combustion interface. Isotope values were measured against calibrated external reference gas. The $\delta^{13}C$ values for individual compounds are reported in the standard delta notation against the Vienna PeeDee Belemnite (VPDB) standard. All samples were run at least in duplicate, with a reproducibility of on average 0.28‰ for the C_{31} *n*-alkane. Precision and accuracy of the squalane internal standard were 0.46‰ and 0.18‰, respectively. The C_{31}

n-alkane is used because it is the most abundant *n*-alkane in sediments from sparsely vegetated regions.

Major-element analysis was carried out using energy-dispersive polarized X-ray fluorescence. We measured 4–8 samples from each timeslice, depending on availability and sedimentation rate, taken at approximately equal spacing. Analytical uncertainty, based on the MAG-1 standard, is less than 1.5% for Al, Si and K and 4% for Ti.

Received 7 October 2010; accepted 16 November 2010; published online 12 December 2010

References

1. Nicholson, S. E. The nature of rainfall variability over Africa on time scales of decades to millenia. *Glob. Planet. Change* **26,** 137–158 (2000).
2. Gasse, F., Chalié, F., Vincens, A., Williams, M. A. J. & Williamson, D. Climatic patterns in equatorial and southern Africa from 30,000 to 10,000 years ago reconstructed from terrestrial and near-shore proxy data. *Quat. Sci. Rev.* **27,** 2316–2340 (2008).
3. Tjallingii, R. *et al.* Coherent high- and low-latitude control of the northwest African hydrological balance. *Nature Geosci.* **1,** 670–675 (2008).
4. Schefuß, E., Schouten, S. & Schneider, R. R. Climatic controls on central African hydrology during the past 20,000 years. *Nature* **437,** 1003–1006 (2005).
5. Tierney, J. E. *et al.* Northern hemisphere controls on tropical southeast African climate during the past 60,000 years. *Science* **322,** 252–255 (2008).
6. Mulitza, S. *et al.* Sahel megadroughts triggered by glacial slowdowns of Atlantic meridional overturning. *Paleoceanography* **23,** PA4206 (2008).
7. deMenocal, P. *et al.* Abrupt onset and termination of the African humid period: Rapid climate responses to gradual insolation forcing. *Quat. Sci. Rev.* **19,** 347–361 (2000).
8. Haug, G. H., Hughen, K. A., Sigman, D. M., Peterson, L. C. & Rohl, U. Southward migration of the intertropical convergence zone through the Holocene. *Science* **293,** 1304–1308 (2001).
9. Yancheva, G. *et al.* Influence of the intertropical convergence zone on the East Asian monsoon. *Nature* **445,** 74–77 (2007).
10. Frierson, D. M. W., Lu, J. & Chen, G. Width of the Hadley cell in simple and comprehensive general circulation models. *Geophys. Res. Lett.* **34,** L18804 (2007).
11. Braconnot, P. *et al.* Results of PMIP2 coupled simulations of the mid-Holocene and Last Glacial Maximum - Part 1: Experiments and large-scale features. *Clim. Past* **3,** 261–277 (2007).
12. Stouffer, R. J. *et al.* Investigating the causes of the response of the thermohaline circulation to past and future climate changes. *J. Clim.* **19,** 1365–1387 (2006).
13. Braconnot, P. *et al.* Results of PMIP2 coupled simulations of the mid-Holocene and Last Glacial Maximum - Part 2: Feedbacks with emphasis on the location of the ITCZ and mid- and high latitudes heat budget. *Clim. Past* **3,** 279–296 (2007).
14. Garcin, Y., Vincens, A., Williamson, D., Buchet, G. & Guiot, J. Abrupt resumption of the African monsoon at the Younger Dryas–Holocene climatic transition. *Quat. Sci. Rev.* **26,** 690–704 (2007).
15. Kim, J. H., Schneider, R. R., Mulitza, S. & Muller, P. J. Reconstruction of SE trade-wind intensity based on sea-surface temperature gradients in the Southeast Atlantic over the last 25 kyr. *Geophys. Res. Lett.* **30,** 2144 (2003).
16. Castaneda, I. S. *et al.* Wet phases in the Sahara/Sahel region and human migration patterns in North Africa. *Proc. Natl Acad. Sci. USA* **106,** 20159–20163 (2009).
17. Maley, J. The African rain forest vegetation and palaeoenvironments during late Quaternary. *Clim. Change* **19,** 79–98 (1991).
18. Schefuß, E., Ratmeyer, V., Stuut, J-B. W., Jansen, J. H. F. & Sinninghe Damsté, J. S. Carbon isotope analyses of *n*-alkanes in dust from the lower atmosphere over the central eastern Atlantic. *Geochim. Cosmochim. Acta* **67,** 1757–1767 (2003).
19. Bird, M. I. *et al.* Terrestrial vegetation change inferred from *n*-alkane δ^{13}C analysis in the marine environment. *Geochim. Cosmochim. Acta* **59,** 2853–2857 (1995).
20. Shanahan, T. M. *et al.* Paleoclimatic variations in West Africa from a record of late Pleistocene and Holocene lake level stands of Lake Bosumtwi, Ghana. *Palaeogeogr. Palaeoclimatol. Palaeoecol.* **242,** 287–302 (2006).
21. Gasse, F. Hydrological changes in the African tropics since the Last Glacial Maximum. *Quat. Sci. Rev.* **19,** 189–211 (2000).
22. Maley, J. Last Glacial Maximum lacustrine and fluviatile formations in the Tibesti and other Saharan mountains, and large-scale climatic teleconnections linked to the activity of the subtropical jet stream. *Glob. Planet. Change* **26,** 121–136 (2000).
23. Salzmann, U. & Waller, M. The Holocene vegetational history of the Nigerian Sahel based on multiple pollen profiles. *Rev. Palaeobot. Palynol.* **100,** 39–72 (1998).
24. Salzmann, U. & Hoelzmann, P. The Dahomey Gap: An abrupt climatically induced rain forest fragmentation in West Africa during the late Holocene. *The Holocene* **15,** 190–199 (2005).
25. Dupont, L. M., Behling, H. & Kim, J-H. Thirty thousand years of vegetation development and climate change in Angola (Ocean Drilling Program Site 1078). *Clim. Past* **4,** 107–124 (2008).
26. Chase, B. M. & Meadows, M. E. Late Quaternary dynamics of southern Africa's winter rainfall zone. *Earth Sci. Rev.* **84,** 103–138 (2007).
27. O'Gorman, P. A. & Schneider, T. The hydrological cycle over a wide range of climates simulated with an idealized GCM. *J. Clim.* **21,** 3815–3832 (2008).
28. Niedermeyer, E. M. *et al.* Orbital- and millennial-scale changes in the hydrologic cycle and vegetation in the western African Sahel: insights from individual plant wax δD and δ^{13}C. *Quat. Sci. Rev.* (in the press) (corrected proof).
29. Still, C. J. & Powell, R. L. in *Isoscapes: Understanding Movement, Pattern, and Process on Earth Through Isotope Mapping* (eds West, J. B., Bowen, G. J., Dawson, T. E. & Tu, K.) (Springer, 2010).

Acknowledgements

We thank A. Govin, H. Renssen and C. Li for comments and discussion. This work was supported by ESF—EUROMARC project 'RETRO' and the DFG Research Centre/Cluster of Excellence 'The Ocean in the Earth System'. AMS dating on the core GeoB9535-4 carried out in Peking University was supported by the NSFC (40776028) and the Fok Ying Tong Education Foundation (111016) and datings carried out in Kiel were supported by the Alexander von Humboldt Foundation.

Author contributions

Experimental work was carried out by J.A.C., E.S., M.Z., R.T., E.H., J.T., A.M. and M.Z. Data analysis and interpretation were carried out by J.A.C., S.M., E.S., D.H., M.P., T.M.D., M.S. and G.W.

Additional information

The authors declare no competing financial interests. Supplementary information accompanies this paper on www.nature.com/naturegeoscience. Reprints and permissions information is available online at http://npg.nature.com/reprintsandpermissions. Correspondence and requests for materials should be addressed to J.A.C.

nature geoscience
SUPPLEMENTARY INFORMATION
DOI: 10.1038/NGEO1039

Modern-day African rainbelt

The African rainbelt is closely associated with the Inter Tropical Convergence Zone (ITCZ). Both oscillate seasonally between ~20°N in July and ~20°S in January (Supplementary Fig. S1a,b) following the seasonal movement of the insolation maximum[S1]. Over West Africa, rainfall is generated by a band of ascending air located between the mid-level African Easterly Jet and the upper-level Tropical Easterly Jet[S2]. Over the Congo basin region, rainfall is associated with the Congolan Air Boundary[S3]. The generation of rainfall and seasonal oscillation of the rainbelt in Africa are also closely linked to the monsoon system[S4], the seasonal reversal of the atmospheric circulation which brings warm moist air on land during the summer.

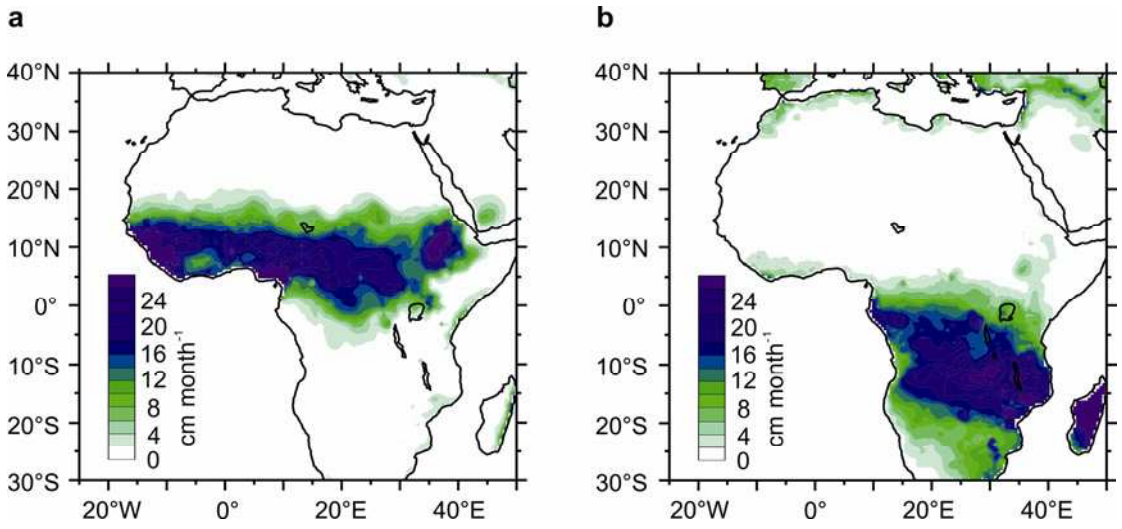

Supplementary Figure S1. Modern-day seasonal extremes of the rainbelt. a, Mean Jun-Jul-Aug precipitation, (cm month^{-1}) for the period 1950-1999 (University of Delaware dataset, http://climate.geog.udel.edu/~climate/). **b,** As (a) but for Dec-Jan-Feb.

DOI: 10.1038/NGEO1039

Estimating wet season length, mean annual rainfall and wet season intensity from vegetation type

In modern-day tropical Africa, mean annual rainfall is controlled by wet season length and wet season intensity. Modern-day $\%C_3$ vegetation is positively correlated with wet season length (Supplementary Fig. S2a), since trees cannot survive when the wet season becomes too short[S5]. Modern-day $\%C_3$ vegetation is also correlated with mean annual rainfall (Supplementary Fig. S2b), owing to the dominance of the spatial distribution of wet season length on the spatial distribution of mean annual rainfall (Fig. 1a,b). Modern-day $\%C_3$ vegetation is weakly correlated with wet season intensity (Supplementary Fig. S2c), suggesting that wet season intensity only exerts a small control on vegetation type.

Since temperature conditions in Africa do not favour the growth of C_3 grasses[S6], changes between C_3 and C_4 vegetation over time represent shifts between trees and grasses and thus represent changes in hydrological conditions, rather than changes in atmospheric CO_2 concentration. Moreover, the large difference in C_3 and C_4 vegetation distribution between the mid-Holocene and late Holocene, when atmospheric CO_2 levels were broadly similar, further emphasises the dominance of hydrological changes (that is changes in wet season length) on changes in C_3 and C_4 vegetation distribution in Africa, rather than changes in atmospheric CO_2 concentration.

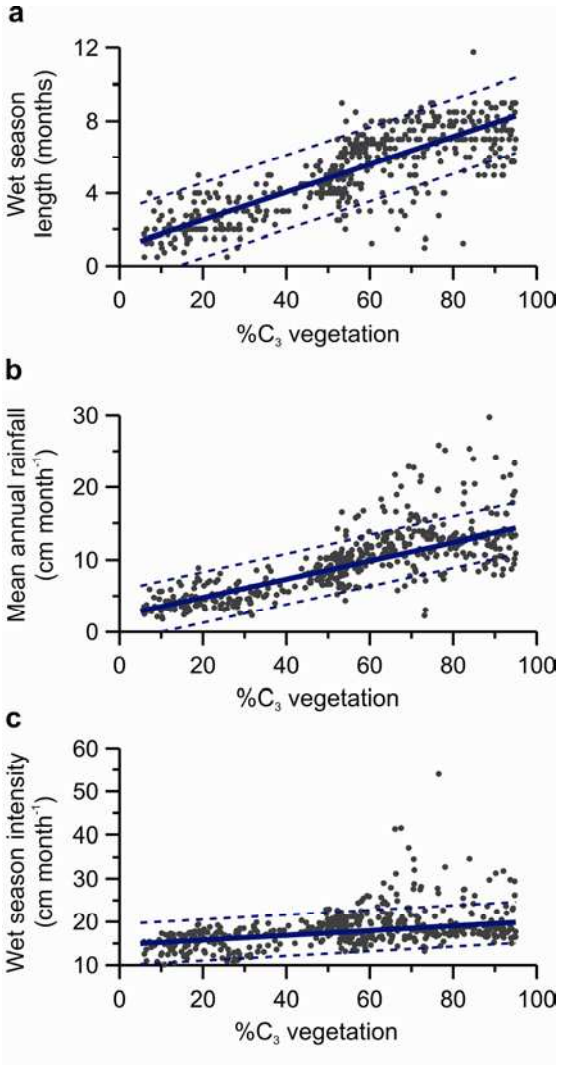

Supplementary Figure S2. $\%C_3$ vegetation as a recorder of wet season length, mean annual rainfall and wet season intensity. **a,** $\%C_3$ vegetation vs. wet season length. Each data point represents the mean value of 1° grid squares for an area extending from the west coast to 20°E, between the latitudes of 20°N to 20°S, for $5\%<C_3<95\%$. The solid line represents a robust linear regression between $\%C_3$ vegetation and wet season length (90% confidence interval is approximately ± 0.1 months). The correlation (r^2) is 0.65 ($p<0.001$). Dashed lines represent the 90% prediction interval. The predictive uncertainty on the regression relationship is ± 2 months. Mean monthly rainfall is based on the University of Delaware dataset, while vegetation type data is based on ref. S7. **b,** As (a) but for $\%C_3$ vegetation vs. mean annual rainfall (90% confidence interval is approximately ± 0.2 cm month^{-1}). The correlation (r^2) is 0.57 ($p<0.001$). The predictive uncertainty on the values is ± 4 cm month^{-1}. **c,** As (a) but for $\%C_3$ vegetation vs. wet season intensity (90% confidence interval is approximately ± 0.3 cm month^{-1}). The correlation (r^2) is 0.18 ($p<0.001$). The predictive uncertainty on the values is ± 5 cm month^{-1}.

DOI: 10.1038/NGEO1039

Transport mechanisms and source areas of material

Most cores receive both river suspended sediment and wind blown dust, although the core at 21°N receives little river material (Fig. 1a), and the cores at 6°S and 12°S receive little dust (Supplementary Fig. S4a). However, the exact location of dust sources are not well known[S8] and neither are the exact areas within river catchments from where cores receive material.

Nonetheless, it is thought that dust storms from the Saharan and Namibian deserts and the Sahel savanna generally follow a westward trajectory[S8,S9]. Apart from the Niger and Congo rivers, major rivers also generally transport material in a westward direction (Fig. 1a). Moreover, during transport and entrainment of a dust storm, the *n*-alkane isotopic composition of the dust source is overprinted with the isotopic composition of the vegetation along the transport pathway[S10], and thus the sediment cores record mostly local vegetation type rather than distal vegetation type. This 'overprinting' by the latest vegetation type is also applicable to material that is transported as river suspended sediment[S11]. Therefore, we assume that the cores at 21-9°N and 12-17°S are receiving their dust and river material from a source area located on the continent approximately eastward of the core site. We assume that the core at 2°30´N receives material mainly from the Sanaga river catchment[S12] and also dust from the Bodelé depression to the north of the core site[S13], while the core at 6°S receives material from the Congo river catchment[S14] (see Fig. 1).

In order to test this assumption of the source areas, we compare the modern-day mean vegetation type (from a satellite-based dataset; ref. S7) of the assumed source areas to the late Holocene vegetation type estimated from the sediment cores. For the cores at 21°N, 15°N, 12°N, 9°N, 12°S, 17°N we calculate the vegetation type from the satellite data for a source area that we designate to be the region 5° of

latitude to the north and south of each core site. A value of 5° is used because the core at 21°N receives material from a region ~5° to the south (there is no vegetation on the adjacent continent; Fig. 1d). Also the latitudinal transport of the Senegal, Balombo, Cunene rivers and any other smaller rivers equates to approximately 5° latitude: therefore the rivers are averaging material from a region 5° to the north and south of the core site. We designate the source area to extend eastwards to 5°W for the cores at 21°N, 15°N, 12°N and 9°N and to 20°E for cores at 12°S and 17°S. For the core at 2°30´N, we designate the source area to be between 15°N and the core site, and between 10°E and 20°E. For the core at 6°S, we designate the Congo River catchment as the area between 5°N and 10°S and between the west coast and 30°E.

In general, the calculated mean $\%C_3$ vegetation for the above designated catchments compares well to the *n*-alkane-derived $\%C_3$ vegetation estimation from the cores for the late Holocene timeslice (Supplementary Fig. S3) and thus implies that this assumption of the source areas is reasonable. Importantly, our source area estimation illustrates that although the source areas are not necessarily centred at the same latitude as the core sites, the combined source area of the whole transect covers the entire latitudinal range of the rainbelt.

DOI: 10.1038/NGEO1039

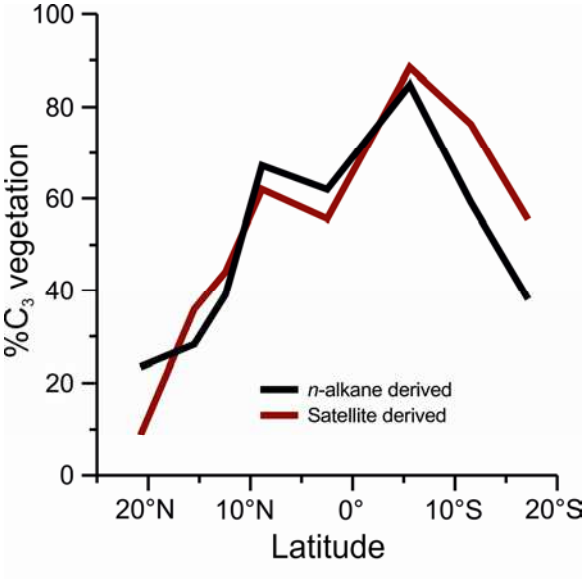

Supplementary Figure S3. Sediment core $\%C_3$ vegetation values compared with estimated continental source area $\%C_3$ vegetation values. Black line represents $\%C_3$ vegetation determined from *n*-alkanes for the late Holocene timeslice of each sediment core, plotted against core site latitude. Red line represents $\%C_3$ vegetation values from the estimated source areas (based on satellite data[S7]) of each core.

Lake Bosumtwi and the 'Dahomey Gap'

Modern-day mean annual rainfall is focussed in the Guinea–Liberia and Cameroon regions, especially in terms of wet season intensity (Fig. 1c) and this is partly related to topography[S15]. In between these two regions lies a savanna corridor known as the 'Dahomey Gap' (Fig. 1d). This is a comparatively dry area (Fig. 1a), in terms of both shorter wet season length (Fig. 1b) and lower wet season intensity (Fig. 1c). These conditions are thought to result from the coastal upwelling of cold waters and the parallel orientation of the south-westerly winds with the coast, which both act to stabilise the lower troposphere and thus reduce rainfall[S16,S17]. Lake Bosumtwi (6°N), which is located adjacent to the Dahomey Gap area, displays low lake levels during the LGM and HS1 relative to today[S18]. This is in contrast to our cores at 9°N (Guinea–Liberia region) and 2°30′N (Cameroon region) which record the same and wetter conditions, respectively. This seems to indicate that the Dahomey Gap region responded differently to the Guinea-Liberia and Cameroon regions during the LGM and HS1.

DOI: 10.1038/NGEO1039

Dust and river proportion

In general, dust is mobilised in arid areas (Supplementary Fig. S4a) and is hence derived from less weathered soils such as Arenosols and Sand dunes[S19] (Supplementary Fig. S4b). Conversely, rivers originate in wet areas (Fig. 1a) and thus derive their material from more heavily weathered soils such as Ferralsols, Nitisols, Acrisols, Plinthosols and Lixisols (Supplementary Fig. S4b). Chemical weathering acts to remove mobile elements such as K and Si[S20], while leaving behind more immobile elements such as Al and Ti[S21-S23]. Therefore, based on the major element composition of the sediment core and of dust, river suspended sediment and marine sediment end-members, we apply an unmixing model to determine the relative proportions of these three components in the sediment[S24]. For the sediment core, samples were measured for major element composition using EDP-XRF analysis. For the end-members, we used 28 values for the major element composition of dust end-members from the northern hemisphere[S20,S25-S29], 9 values for dust from the southern hemisphere[S30] and 13 values for river suspended sediment from the Senegal, Niger and Congo Rivers[S23,S31-S33]. The marine end member was constructed using the same assumptions as in ref. S24.

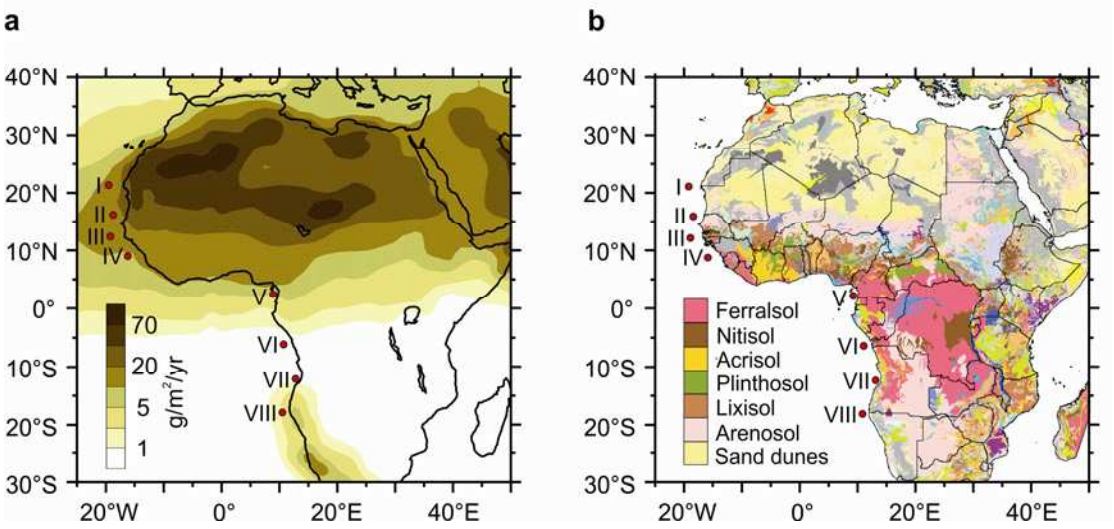

Supplementary Figure S4a. Modern-day average dust deposition across Africa[S34,S35] (g/m^2/yr). A large amount dust is transported to the west from the Sahara-Sahel region and a smaller amount from the Namib/Kalahari deserts. **b, Major soil groups across Africa[S36].** Heavily weathered soils include Ferralsols, Nitisols, Acrisols, Plinthosols and Lixisols. Less weathered soil groups include Arenosols and Sand dunes. Soil groups not given in the key are those that are defined on properties not linked to climate.

The bootstrapping method used in the unmixing analysis incorporates some of the uncertainty in possible end member composition into the final unmixing model[S24]. However, the limited availability of both dust and river end members, particularly for the southern hemisphere, restricts the ability of the model to fully characterise the end member composition of each source area and thus to quantitatively determine the amount of each component in each core. Nonetheless, we are still able to qualitatively estimate relative changes in dust/river ratio between each timeslice.

We present the results as dust proportion divided by river proportion (Supplementary Fig. S5). The dust flux to the core site is thought to be dependent on aridity[S24] and also wind strength[S37]. River flux is mostly dependant on continental aridity, since total suspended sediment discharge increases with annual water

DOI: 10.1038/NGEO1039

discharge[S38]. The magnitude of the increase in dust/river at the LGM and HS1 is much greater in the 21-12°N region than in other regions (Supplementary Fig. S5). This perhaps reflects a greater potential for dust mobilisation in the Sahara-Sahel region than in central and southern Africa.

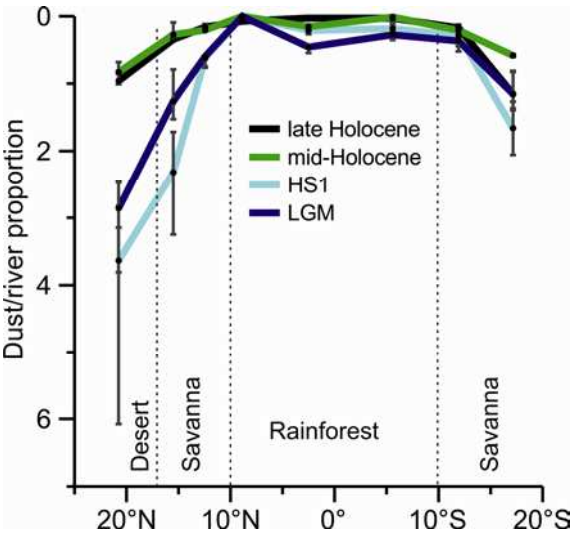

Supplementary Figure S5. Latitudinal distribution of dust/river ratio for modern and past climate states. Dust proportion divided by river proportion plotted against core-site latitude for the LGM (19-23ka), HS1 (16-19ka), mid-Holocene (6-8ka) and late Holocene (0-2ka). Each data point is the median value of the unmixing iterations for each sample from each timeslice. Error bars are nonparametric 95% confidence intervals, and represent the variation between each of the unmixing iterations for each sample as well as the variability between samples within any given timeslice.

Seasonal oscillation, latitudinal width and intensity of the rainbelt

In terms of rainbelt dynamics, the distribution of wet season length on the continent is controlled by the latitudinal extent of the seasonal oscillation of the rainbelt, and also by the latitudinal width of the rainbelt (that is the width of the band of rain during a given part of the year). A reduction in seasonal oscillation would produce a contraction of the rainbelt, while a reduction in the latitudinal width of the rainbelt would result in a reduction in wet season length across all latitudes. In addition, although the correlation is poor (Supplementary Fig. S2c), the intensity of the rainbelt (that is the wet season intensity) may also exert some control on vegetation type: for example there may be a lower limit of wet season intensity that is required to sustain rainforest. A reduction in wet season intensity would result in a reduction in mean annual rainfall across all latitudes.

Chronology

Age models for GeoB9508-5, GeoB9526-4/5, GeoB4905-4, GeoB6518-1, ODP1078C and GeoB1023-5 are based on published chronologies[S12,S14,S39-S44]. The age models for GeoB7920-2 and GeoB9535-4 are based on new AMS ^{14}C ages (Supplementary Table S1). Calibration was performed with the 'Fairbanks 0107' calibration curve[S45], using a reservoir age of 400 yrs.

DOI: 10.1038/NGEO1039

Supplementary Table S1: ^{14}C-AMS Dates used for chronology of GeoB7920-2 and GeoB9535-4

		Radiocarbon age		Calendar age	
Sample	Depth (cm)	Mean (yr BP)	1 std dev (yr BP)	Mean (yr BP)	1 std dev (yr BP)
GeoB7920-2					
KIA 35956	3	500	35	523	16
KIA 35955	53	4215	60	4788	80
KIA 35954	103	7410	90	8232	98
KIA 35953	148	9130	110	10286	120
KIA 35951	193	11700	70	13562	78
KIA 35950	228	12580	80	14624	153
KIA 35949	268	16320	110	19439	122
KIA 35948	298	19700	160	23533	224
GeoB9535-4					
KIA 35171	2	1000	30	923	24
BA081346†	5	2225	35	2246	63
BA081347†	16	6810	40	7646	31
BA081348†	23	9295	55	10493	80
BA081349†	29	10390	40	12247	103
KIA 35170	40	12250	100	14052	139
BA081350†	41	12430	60	14332	146
BA081351†	51	14080	45	16452	128
BA081352†	63	14415	45	16979	128
BA081353†	83	16120	50	19249	87
BA081354†	107	17610	55	20830	108
BA081355†	129	18855	60	22432	82
BA081356†	147	21100	65	25257	117
BA081357†	167	22735	75	27307	158
BA081358†	181	24290	80	29058	150
BA081359†	193	25145	75	30271	153
KIA35169	194	25800	+510/-480	30999	598
BA081360†	223	29165	100	34583	173
KIA35168	254	36670	+2120/-1680	41801	1913

†Measured at Peking University, all others measured at Kiel University

References

S1 Nicholson, S. E. The nature of rainfall variability over Africa on time scales of decades to millenia. *Global Planet. Change* **26,** 137-158 (2000).

S2 Nicholson, S. E. A revised picture of the structure of the "monsoon" and land ITCZ over West Africa. *Clim. Dyn.* **32,** 1155-1171 (2009).

S3 Leroux, M. *Le climat de L'Afrique tropicale*. (Paris, 1983).

S4 Trenberth, K. E., Stepaniak, D. P., and Caron, J. M. The Global Monsoon as Seen through the Divergent Atmospheric Circulation. *J. Clim* **13,** 3969-3993 (2000).

S5 Maley, J. The African rain forest vegetation and palaeoenvironments during late Quaternary. *Clim. Change* **19,** 79-98 (1991).

S6 Edwards, E. J., Osborne, C. P., Stromberg, C. A. E., Smith, S. A., and Consortium, C. G. The Origins of C4 Grasslands: Integrating Evolutionary and Ecosystem Science. *Science* **328,** 587-591 (2010).

S7 Still, C. J. and Powell, R. L., *Continental-scale distributions of plant stable carbon isotopes* in *Isoscapes: Understanding movement, pattern, and process on Earth through isotope mapping*, Edited by J. B. West, Bowen, G.J., Dawson, T.E., and K. Tu (Springer, Dordrecht, 2010).

S8 Goudie, A. S. and Middleton, N. J. Saharan dust storms: nature and consequences. *Earth Sci. Rev.* **56,** 179-204 (2001).

S9 Stuut, J.-B. W. et al. A 300-kyr record of aridity and wind strength in southwestern Africa: inferences from grain-size distributions of sediments on Walvis Ridge, SE Atlantic. *Marine Geology* **180,** 221-233 (2002).

S10 Simoneit, B. R. T., Cox, R. E., and Standley, L. J. Organic matter of the troposphere--IV. Lipids in Harmattan aerosols of Nigeria. *Atmos. Environ.* **22,** 983-1004 (1988).

S11 Bouillon, S. et al. Distribution, origin and cycling of carbon in the Tana River (Kenya): a dry season basin-scale survey from headwaters to the delta. *Biogeosciences* **6,** 2475-2493 (2009).

S12 Weldeab, S., Schneider, R. R., Kolling, M., and Wefer, G. Holocene African droughts relate to eastern equatorial Atlantic cooling. *Geology* **33,** 981-984 (2005).

S13 Stuut, J.-B. et al. Provenance of present-day eolian dust collected off NW Africa. *J. Geophys. Res.* **110,** D04202 (2005).

S14 Schefuß, E., Schouten, S., and Schneider, R. R. Climatic controls on central African hydrology during the past 20,000 years. *Nature* **437,** 1003-1006 (2005).

S15 Sall, S. M., Viltard, A., and Sauvageot, H. Rainfall distribution over the Fouta Djallon - Guinea. *Atmos. Res.* **86,** 149-161 (2007).

S16 Hayward, D. F. and Oguntoyinbo, J. S. *The climatology of West Africa* (Hutchinson, Barnes & Noble, London, Totowa, 1987).

S17 Vollmert, P., Fink, A. H., and Besler, H. Ghana Dry Zone und Dahomey Gap: Ursachen fuer eine Niederschlagsanomalie im tropischen Westafrika. *Beitr. Phys. Geogr.* **4,** 375-393 (2003).

DOI: 10.1038/NGEO1039

S18 Shanahan, T. M. et al. Paleoclimatic variations in West Africa from a record of late Pleistocene and Holocene lake level stands of Lake Bosumtwi, Ghana. *Palaeogeogr. Palaeoclimatol. Palaeoecol.* **242,** 287-302 (2006).

S19 Driessen, P. M., Deckers, J. A., Spaargaren, O. C., and Nachtergaele, F. O. *Lecture Notes on the Major Soils of the World*. (Food and Agriculture Organization of the United Nations, Rome, 2001).

S20 Moreno, T. et al. Geochemical variations in aeolian mineral particles from the Sahara-Sahel Dust Corridor. *Chemosphere* **65,** 261-270 (2006).

S21 Middelburg, J. J., van der Weijden, C. H., and Woittiez, J. R. W. Chemical processes affecting the mobility of major, minor and trace elements during weathering of granitic rocks. *Chem. Geol.* **68,** 253-273 (1988).

S22 Zabel, M. et al. Late Quaternary Climate Changes in Central Africa as Inferred from Terrigenous Input to the Niger Fan. *Quaternary Research* **56,** 207-217 (2001).

S23 Gaillardet, J., Dupré, B., and Allègre, C. J. Geochemistry of large river suspended sediments: silicate weathering or recycling tracer? *Geochim. Cosmochim. Acta* **63,** 4037-4051 (1999).

S24 Mulitza, S. et al. Increase in African dust flux at the onset of commercial agriculture in the Sahel region. *Nature* **466,** 226-228 (2010).

S25 Wilke, B. M., Duke, B. J., and Jimoh, W. L. O. Mineralogy and chemistry of Harmattan dust in Northern Nigeria. *Catena* **11,** 91-96 (1984).

S26 Orange, D. and Gac, J. Y. Bilan géochimique des apports atmosphériques en domaines sahélien et soudano-guinéen d'Afrique de l'Ouest (bassins supérieurs du Sénégal et de la Gambie). *Géodynamique* **5,** 51-65 (1990).

S27 Orange, D., Gac, J. Y., and Diallo, M. I. Geochemical assessment of atmospheric deposition including Harmattan dust in continental west Africa *Tracers in Hydrology (Proceedings of the Yokohama Symposium, July 1993) IAMS Publ. no. 215,* 303-312 (1993).

S28 Guieu, C. and Thomas, A. J., *Saharan aerosols: from the soil to the ocean* in *The impact of desert dust across the Mediterranean*, Edited by S. Guerzoni and R. Chester (Kluwer, Amsterdam, 1996).

S29 Nguetnkam, J. P., Kamga, R., Villiéras, F., Ekodeck, G. E., and Yvon, J. Altération différentielle du granite en zone tropicale. Exemple de deux séquences étudiées au Cameroun (Afrique centrale). *Comptes Rendus Geosciences* **340,** 451-461 (2008).

S30 ISRIC Soil Information System (ISIS) http://isis.isric.org/.

S31 Gac, J. Y. and Kane, A. Le fleuve Sénégal: I. Bilan hydrologique et flux continentaux de matières particulaires à l'embouchure. *Sciences Géologiques Bulletin* **39,** (1986).

S32 Martin, J.-M. and Meybeck, M. Elemental mass-balance of material carried by major world rivers. *Mar. Chem.* **7,** 173-206 (1979).

S33 Sholkovitz, E. R., van Grieken, R., and Eisma, D. The major-element composition of suspended matter in the Zaire river and estuary. *Netherlands Journal of Sea Research* **12,** 407-413 (1978).

S34 Mahowald, N. M. et al. Atmospheric global dust cycle and iron inputs to the ocean. *Global Biogeochem. Cycles* **19,** (2005).

S35 Jickells, T. D. et al. Global Iron Connections Between Desert Dust, Ocean Biogeochemistry, and Climate. *Science* **308,** 67-71 (2005).

S36 FAO/IIASA/ISRIC/ISSCAS/JRC. *Harmonized World Soil Database (version 1.1)*. (FAO, Rome, Italy and IIASA, Laxenburg, Austria., 2009).

S37 Ruddiman, W. F. Tropical Atlantic terrigenous fluxes since 25,000 yrs B.P. *Marine Geology* **136,** 189-207 (1997).

S38 Coynel, A., Seyler, P., Etcheber, H., Meybeck, M., and Orange, D. Spatial and seasonal dynamics of total suspended sediment and organic carbon species in the Congo River. *Global Biogeochem. Cycles* **19,** GB4019 (2005).

S39 Kim, J. H., Schneider, R. R., Mulitza, S., and Muller, P. J. Reconstruction of SE trade-wind intensity based on sea-surface temperature gradients in the Southeast Atlantic over the last 25 kyr. *Geophys. Res. Lett.* **30,** 2144, doi: 2110.1029/2003GL017557 (2003).

S40 Kim, J.-H., Schneider, R. R., Müller, P. J., and Wefer, G. Interhemispheric comparison of deglacial sea-surface temperature patterns in Atlantic eastern boundary currents. *Earth Planet. Sci. Lett.* **194,** 383-393 (2002).

S41 Adegbie, A. T., Schneider, R. R., Röhl, U., and Wefer, G. Glacial millennial-scale fluctuations in central African precipitation recorded in terrigenous sediment supply and freshwater signals offshore Cameroon. *Palaeogeogr. Palaeoclimatol. Palaeoecol.* **197,** 323-333 (2003).

S42 Mulitza, S. et al. Sahel megadroughts triggered by glacial slowdowns of Atlantic meridional overturning. *Paleoceanography* **23,** PA4206 (2008).

S43 Dupont, L. M., Behling, H., and Kim, J.-H. Thirty thousand years of vegetation development and climate change in Angola (Ocean Drilling Program Site 1078). *Clim. Past* **4,** 107-124 (2008).

S44 Zarriess, M. and Mackensen, A. The tropical rainbelt and productivity changes off northwest Africa: A 31,000-year high-resolution record. *Marine Micropaleontology* **76,** 76-91 (2010).

S45 Fairbanks, R. G. et al. Radiocarbon calibration curve spanning 0 to 50,000 years BP based on paired Th-230/U-234/U-238 and C-14 dates on pristine corals. *Quat. Sci. Rev.* **24,** 1781-1796 (2005).